Electronic Supplementary Information (ESI):

Cyclic polymers with pendant triphenylene discogens: convenient synthesis and topological effect on thermotropic liquid crystal behavior and fluorescence enhancement†

Bin Mu,[a] Qian Li,[a] Xiao Li,[a] Shi Pan,[a] Yang Zhou,[a] Jianglin Fang,[b] and Dongzhong Chen*,[a]

[a] *Key Laboratory of High Performance Polymer Materials and Technology of Ministry of Education, Collaborative Innovation Center of Chemistry for Life Sciences, Department of Polymer Science and Engineering, School of Chemistry and Chemical Engineering, Nanjing University, Nanjing 210023, China.*

E-mail: cdz@nju.edu.cn

[b] *Center for Materials Analysis, Nanjing University, Nanjing 210093, China.*

Table of Contents

1. Materials and measurements

Materials

The synthesis of monomers **1**(*m*) was carried out according to our previously reported procedure.[1,2] The reagents 3-bromo-1-propanol (>93%, TCI), sodium azide (A. R.), carbon disulfide (99.9%, Alfa-Aesar), 3-butyn-1-ol (>97%, TCI) and 2-bromopropiomyl bromide (97%, Sigma-Aldrich) were used as received. Triethylamine (99%) was refluxed over calcium hydride and freshly redistilled before use. Dichloromethane (CH_2Cl_2) was refluxed over calcium hydride and distilled before use. The 1,4-dioxane was refluxed over sodium/benzophenone until the solution turned purple and distilled before use. The 2,2-azobis(isobutyronitrile) (AIBN, 99%) was recrystallized twice from ethanol and dried under vacuum at room temperature. All other chemical reagents were commercially available and used as received.

Measurements

1D ^{1}H NMR spectra in solution were obtained from 300 MHz (Bruker DRX 300) and 500 MHz (Bruker DRX 500) instruments, and 2D ^{1}H NMR spectra were recorded on a Bruker Avance III 400 spectrometer. Fourier transform infrared spectra (FT-IR) were recorded on a NICOLET iS10 infrared spectrometer. Mass spectra were recorded on a LCMS-2020 single quadrupole equipped with electrospray ionization (ESI) source interface (Shimadzu). Matrix-assisted laser desorption/ionization time-of-flight mass spectrometry (MALDI-TOF-MS) were performed on an MALDI TOF-TOF 4800 plus (ABSCIEX) instrument. Gel permeation chromatography (GPC) measurements were performed at 25 ℃ on a Waters 515 system equipped with Wyatt Technology Optilab rEX differential refractive index and UV detectors. THF was used as the eluent at a flow rate of 1.0 mL min^{-1}, the solvent THF and sample solutions were filtered over filters with pore size of 0.45 μm (Nylon, Millex-HN 13 mm Syringes Filters, Millipore, US). Relative weight average (M_w) and number average (M_n) molecular weights were calculated with a calibration curve based on a group of polystyrene standard samples. Ultraviolet visible (UV-vis) spectra were recorded on a Shimadzu UV-3600 spectrometer. Fluorescence spectra were recorded with a HORIBA Jobin Yvon FM-4NIR spectrofluorometer.

Differential scanning calorimetry (DSC) thermograms were recorded on a Perkin-Elmer Pyris I

calorimeter equipped with a cooling accessory and under an argon atmosphere. Typically, about 8 mg of the solid sample was encapsulated in a sealed aluminum pan with an identical empty pan as the reference. Indium was used as a calibration standard. The polarized optical microscopy (POM) was adopted to observe thermal transitions and take texture photographs with a PM6000 microscope under cross-polarizers equipped with a Leitz-350 heating stage and an associated Nikon (D3100) digital camera. The samples were prepared by melt-pressing and sandwiched between two glass plates. X-ray scattering experiments were performed with a high-flux small-angle X-ray scattering instrument (SAXSess mc^2, Anton Paar) equipped with Kratky block-collimation system and a temperature control unit (Anton Paar TCS 120 and TCS 300). Both small angle X-ray scattering (SAXS) and wide angle X-ray scattering (WAXS) were simultaneously recorded on an imaging-plate (IP) with extended angle range (the q range covered by the IP was from 0.06 to 29 nm^{-1}, $q = 4\pi\sin\theta/\lambda$, where the wavelength λ is 0.1542 nm of Cu-Kα radiation and 2θ is the scattering angle) at 40 kV and 50 mA. The powder samples were encapsulated with aluminum foil during the measurement and the obtained X-ray analysis data were processed with the associated SAXSquant software 3.80 and the aluminum foil background signal was subtracted.

2. Synthesis of *α, ω*–heterodifunctional chain transfer agent (*df*-CTA)

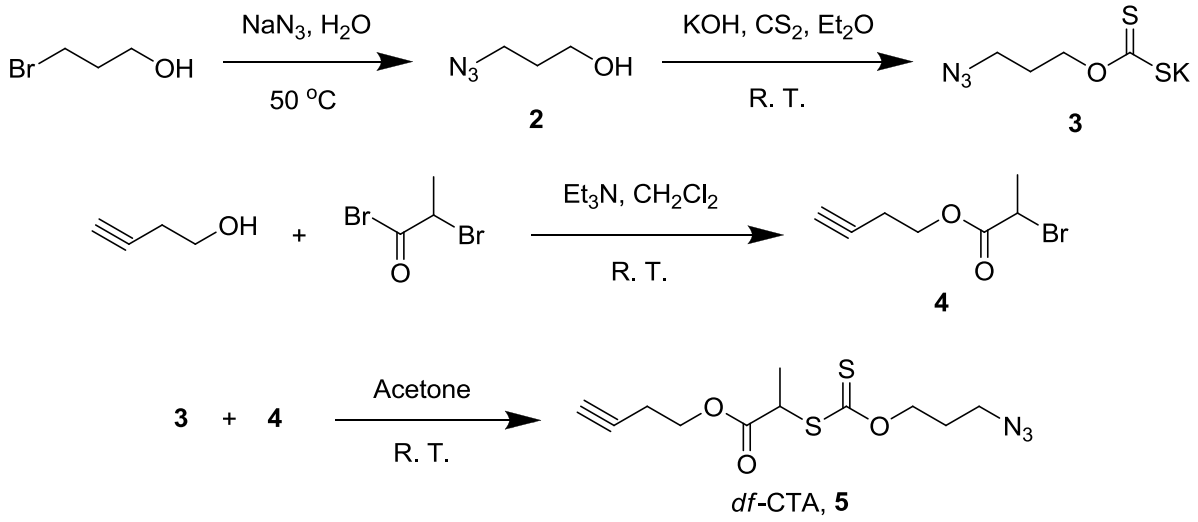

Scheme S1. Synthetic route of *α, ω*–heterodifunctional chain transfer agent (*df*-CTA, **5**)

3-azidopropan-1-ol (**2**)**.** This compound was prepared according to the literature procedure.[3] A mixed solution of 3-bromo-1-propanol (2.15 g, 15.5 mmol) and sodium azide (2.1 g, 32.3 mmol) in 15 mL deionized water was heated to 50 ℃ and stirred for 40 h. After cooling, the mixture was extracted with dichloromethane. Then the combined organic layers were washed with concentrated sodium chloride solution, dried over anhydrous magnesium sulfate, filtered and concentrated under reduced pressure to obtain 1.2 g **2** in colorless oil (yield 77%). ^{1}H NMR (300 MHz, $CDCl_3$) δ (ppm): 3.77 (t, 2H, *J* = 6.0 Hz, C*H*$_2$OH), 3.46 (t, 2H, *J* = 6.6 Hz, CH_2N_3), 1.84 (m, 2H, $CH_2CH_2CH_2$).

Potassium *O*-3-azidopropyl xanthate (**3**)**.** This compound was carried out according to a modified literature procedure.[4,5] **2** (1.2 g, 11.8 mmol) in 50 mL anhydrous ether was treated with freshly crushed potassium hydroxide (0.66 g, 11.8 mmol) and carbon disulfide (0.8 mL, 13.0 mmol) and subsequently stirred at 30 ℃ for 4 h. The crude product in light yellow precipitate was collected by filtration, and then dissolved in acetone and filtered, after adding proper amount of anhydrous ether and the precipitate was collected and dried to obtain the final product **3** 0.97 g in light yellow solid (yield 38%). ^{1}H NMR (300 MHz, dimethylsulfoxide-d_6) δ (ppm): 4.25 (t, 2H, *J* = 6.5 Hz, CH_2O), 3.40 (t, 2H, *J* = 6.9 Hz, CH_2N_3), 1.86 (m, 2H, $CH_2CH_2CH_2$).

But-3-ynyl 2-bromopropanoate (**4**)**.** A mixed solution of 3-butyn-1-ol (2.1 g, 30.0 mmol) and triethylamine (6.0 mL, 43.1 mmol) in 40 mL dichloromethane was prepared, under a nitrogen atmosphere in ice-water bath, and then 2-bromopropionyl bromide (4.5 mL, 42.9 mmol) was added slowly. After addition the mixture was stirred for 30 min at around 0 ℃ and then continued for 4 h at room temperature. After filtered to remove residue salt, washed with water, and dried over anhydrous magnesium sulfate, then separated through silica-gel column chromatography using mixed solvents of petroleum ether / dichloromethane (3 : 1, v/v), the final product 4.4 g was obtained in colorless liquid (yield 72%). ^{1}H NMR (300 MHz, $CDCl_3$) δ (ppm): 4.40 (q, 1H, *J* = 7.0 Hz, C*H*CH_3), 4.29 (t, 2H, *J* = 6.8 Hz, CH_2O), 2.59 (m, 2H, C*H*$_2CH_2O$), 2.03 (t, 1H, *J* = 2.6 Hz, C*H*CCH_2), 1.84 (d, 3H, *J* = 7.0 Hz, C*H*$_3CH$).

Buty-3-nyl 2-((4-azidobutoxy)carbonothioylthio)propanoate, *df*-CTA (5). A mixture of **3** (0.97 g, 4.5 mmol) and **4** (0.82 g, 4.0 mmol) in 10 mL acetone was stirred at room temperature overnight. After filtered off the precipitate, the acetone was removed under reduced pressure, the crude product was dissolved in dichloromethane, washed with water, dried over anhydrous magnesium sulfate, and finally purified via silica-gel column chromatography using petroleum ether / ethyl acetate (20 : 1, v/v) as the eluent. After dried 0.9 g yellow oil product was obtained (yield 75%). ^{1}H NMR (300 MHz, $CDCl_3$) δ (ppm): 4.66 (t, 2H, *J* = 6.1 Hz, $CH_2OC(S)$), 4.40 (q, 1H, *J* = 7.2 Hz, C*H*CH_3), 4.27 (t, 2H, *J* = 6.8 Hz, $CH_2OC(O)$), 3.47 (t, 2H, *J* = 6.7 Hz, CH_2N_3), 2.57 (m, 2H, C*H*$_2$CCH), 2.07 (m, 2H, C*H*$_2$$CH_2N_3$), 2.01 (t, 1H, *J* = 2.7 Hz, C*H*CCH_2), 1.60 (d, 3H, *J* = 7.2 Hz, C*H*$_3$CH). ESI-MS (*m/z*): [M + H]$^+$ calcd for $C_{11}H_{16}N_3O_3S_2$, 302.06; found, 302.10. [M + NH_4]$^+$ calcd for $C_{11}H_{19}N_4O_3S_2$, 319.09; found, 319.10.

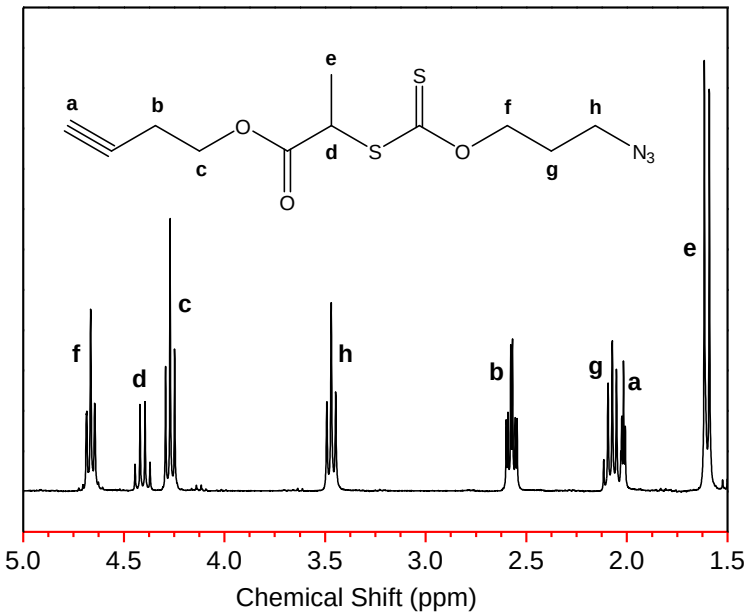

Figure S1. ^{1}H NMR (300 MHz, $CDCl_3$) spectrum of *df*-CTA, **5**

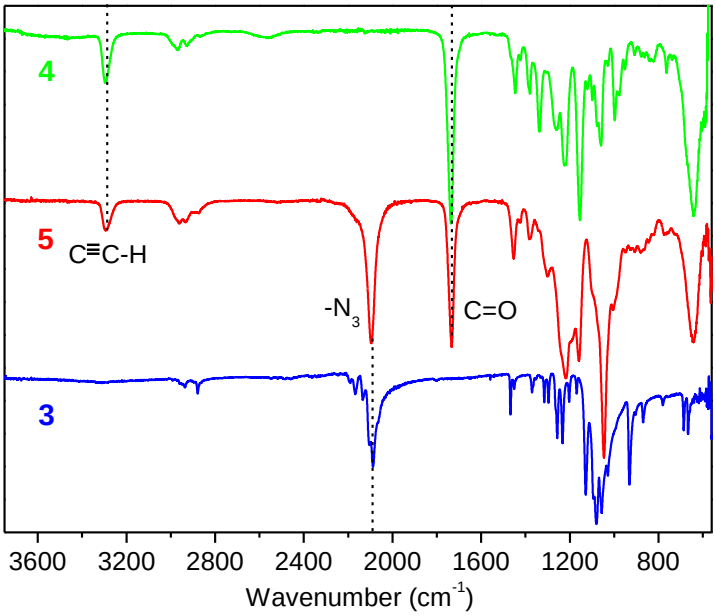

Figure S2. FT-IR spectra comparison of *df*-CTA (**5**) and its reactive intermediates **3** and **4**

3. Controlled preparation of cyclic polymers with pendant triphenylene discogens

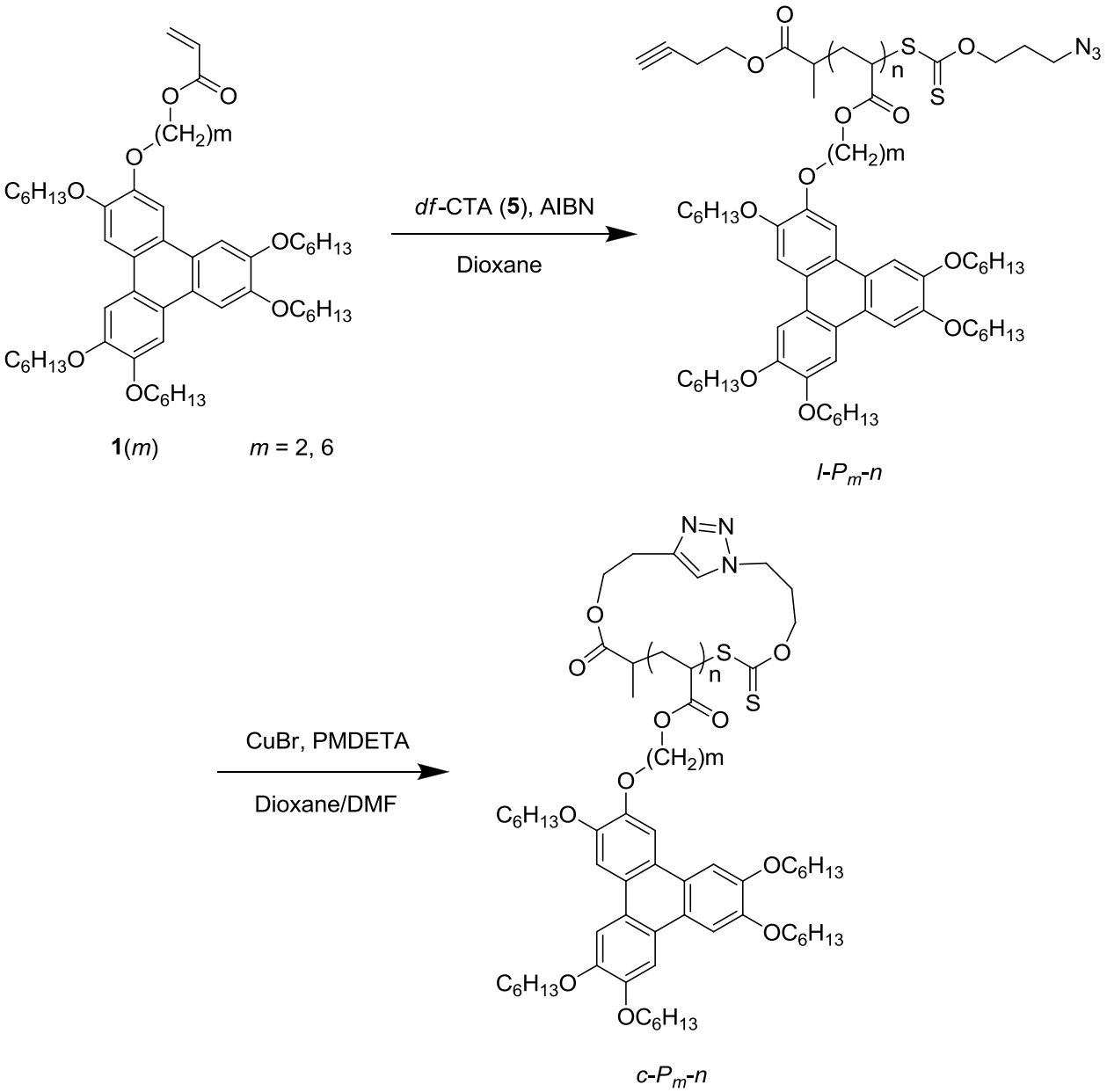

1(*m*) *m* = 2, 6

l-P_m-*n*

c-P_m-*n*

Scheme S2. Synthesis of cyclic polymers *c*-P_m-*n* by a combination of RAFT polymerization with *df*-CTA (**5**) as the chain transfer agent and copper catalyzed azide-alkyne click cyclization.

Reaction kinetics study of RAFT polymerization of monomer 1(6) via *df*-CTA (designed DP 20). Monomer **1**(6) (0.3565 g, 0.40 mmol), AIBN (0.81 mg, 0.0050 mmol), *df*-CTA (**5**, 5.96 mg, 0.02 mmol), and dioxane (0.70 mL) were added into a 10 mL Schlenk flask and degassed via freeze-pump-thaw cycle three times. The flask was heated in a 60 ℃ oil bath. Starting from reaction for 2 h, 20 μL of the reaction mixture was sampled in a certain time interval with a 100 μL microsyringe, which was equipped with a long needle and filled with ultrahigh purity nitrogen

atmosphere. After transferred into a clean NMR tube, the taken sample drop was immediately frozen with liquid nitrogen and exposed to air atmosphere to quench polymerization. After removing solvent under vacuum and then adding 0.6 mL deuterated chloroform, the reaction mixture solution was analyzed with 500 MHz high resolution ^{1}H NMR and the conversion percentage was estimated quantitatively based on integral area ratio of characteristic signals as described in our previous paper.[1] The kinetics plot was obtained as shown in Figure S3 demonstrating well linear fitting of conversion versus polymerization time.

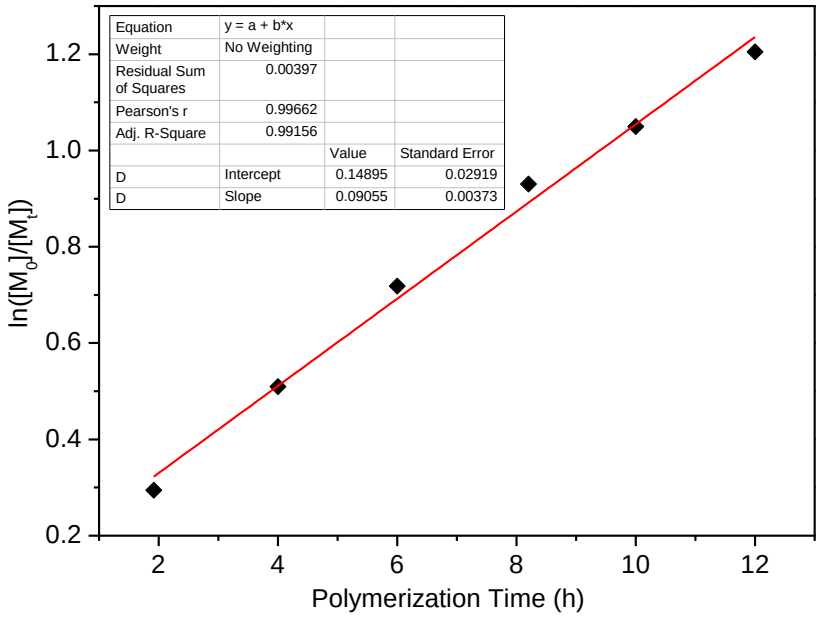

Figure S3. Kinetics plot of the RAFT polymerization (designed DP 20) showing very good linear fitting of conversion vs polymerization time.

Synthesis of precursor linear polymer *l*-P_6-10. The polymerization was conducted according to the same procedure as described in kinetics study, while the reaction time was chosen to be 7 h at a 50% conversion for the designed DP 10 sample. The polymer product was separated and purified through silica-gel column chromatography with the same protocol adopted in the previous paper for linear homopolymers.[1] The final polymer was harvested in yield 48.3% very close to the theoretical value.

Synthesis of cyclic polymer *c*-P_6-10. A mixed solution of 200 mL DMF and 100 mL dioxane in 500 mL three-necked flask was degassed via freeze-pump-thaw cycle, then under nitrogen atmosphere cuprous bromide (0.7 g, 4.9 mmol) and N,N,N′,N′,N″-pentamethyldiethylenetriamine (PMDETA, 1.0

mL, 4.9 mmol) were added. A mixed solution of precursor *l*-P_6-10 (0.2049 g) in 60 mL DMF and 60 mL dioxane was added very slowly by using a pressure-equalizing dropping funnel over 48 h at 90 ℃ then the mixture was continuing to react for another 24 h. After removal of dioxane and DMF, the crude product was dissolved in dichloromethane and washed with water four times, finally purified by neutral alumina column chromatography with ethyl acetate as the eluent to obtain 0.125 g solid product in light yellow (yield 61%).

The other cyclic polymers *c*-P_6-18 and *c*-P_2-10 and their corresponding linear polymer precursors *l*-P_6-18 and *l*-P_2-10 were prepared similarly with above described procedures.

4. Molecular characterization comparison of cyclic polymers *c*-P_m-*n* with linear counterparts *l*-P_m-*n*

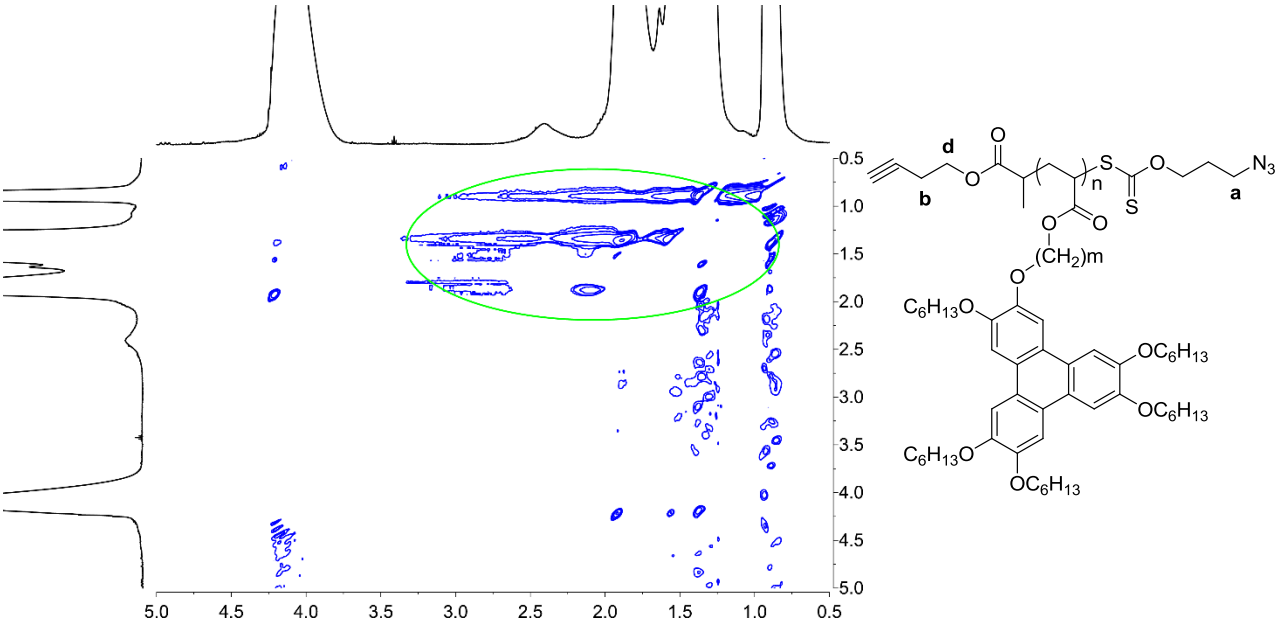

Figure S4. 2D NOESY spectrum of *l*-P_6-10 in $CDCl_3$

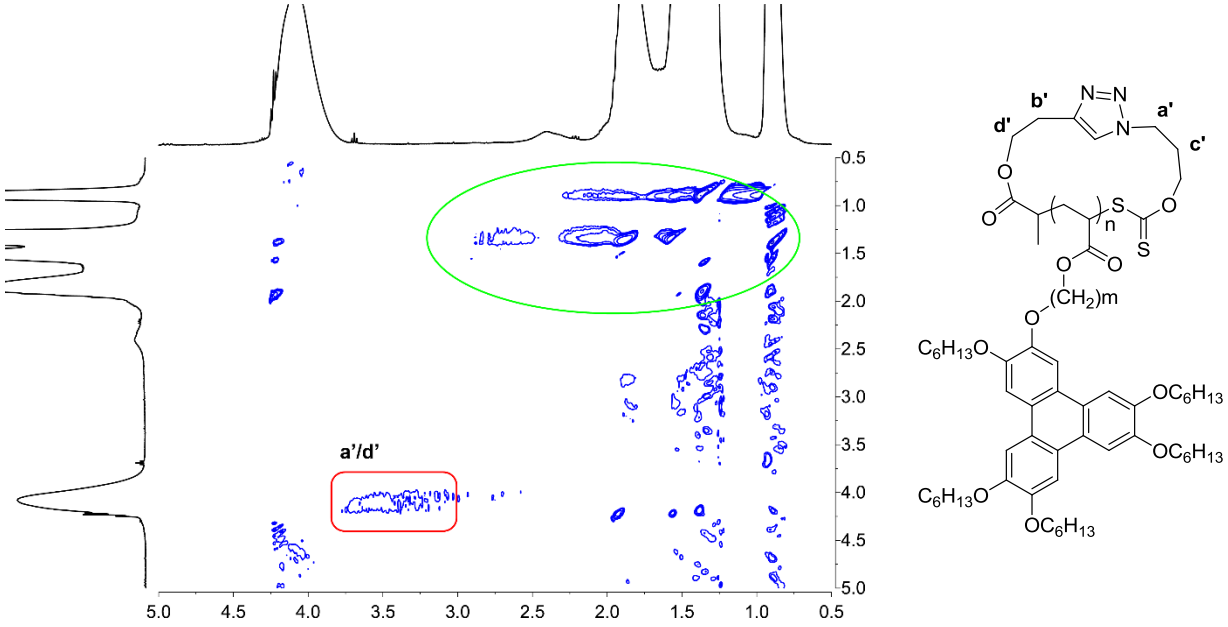

Figure S5. 2D NOESY spectrum of *c*-P_6-10 in $CDCl_3$

The successful preparation of cyclic polymers was verified with ^{1}H NMR, FT-IR and GPC characteriztion (Figure 2 in the main text), and also further corroborated by advanced 2D NMR technique with nuclear overhauser effect spectroscopy (NOESY) to discriminate the spatial conformational structure. As shown in Figure S4 and Figure S5, besides some differences reflecting the variant position aliphatic protons as indicated by an green oval, an additional cross peak emerged in the spectrum of *c*-P_6-10 as highlighted by a red rectangle in Figure S5, which can be attributed to the spatial proximity of CH_2(**a′**) and CH_2(**d′**) of cyclic polymer *c*-P_6-10 as compared with its linear precursor *l*-P_6-10.

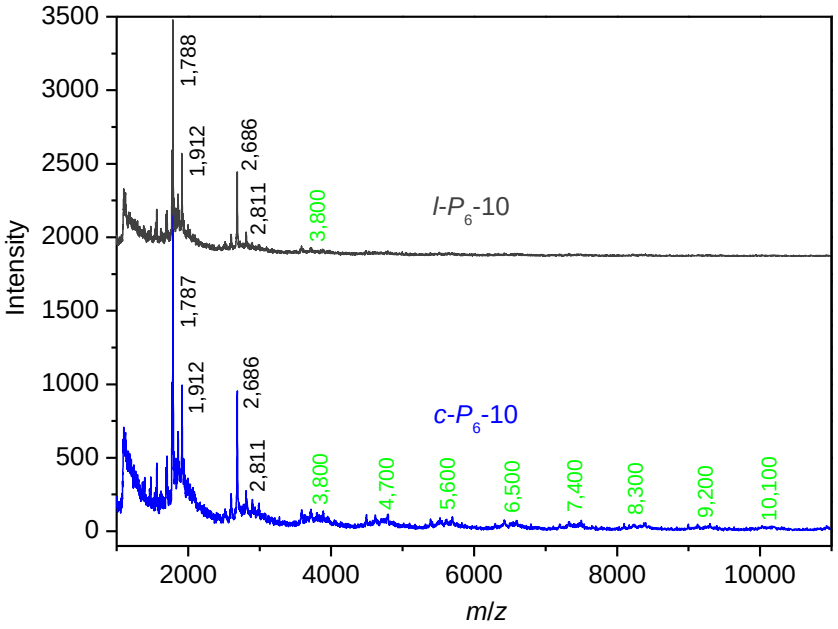

Figure S6. MALDI-TOF-MS patterns comparison of the linear precursor *l*-P_6-10 and cyclic polymer *c*-P_6-10 with dithranol as the matrix, with the *m/z* numbers in black denoting precise values of partly line-resolved patterns, while those in green for median values of the corresponding group peaks of lower intensity. The profile of *l*-P_6-10 has been offset along the vertical axis.

The MALDI-TOF-MS analyses have been performed with the dithranol matrix as previously adopted for the homologous side-chain discotic LC polymers (P_6-*n*).[1] Although not line-resolved MALDI-TOF-MS profiles were obtained, the results gave some essential difference between cyclic and linear polymers. As shown in Figure S6, both *c*-P_6-10 and *l*-P_6-10 displayed a series similar fragmented ionic peaks with corresponding peak intervals of adjacent groups were almost constant and approximate to the molar mass 899 g mol^{-1} of discotic TP acrylate repeat unit, indicating fragmentation occurred during the MALDI fracture process as previously revealed.[1] Despite the main strong peaks of both *c*-P_6-10 and *l*-P_6-10 locating at less than 3,000 Da looked quite similar, while the cyclic polymer *c*-P_6-10 showed many groups of weak peaks in the higher molecular weight range 3,000~11,000 Da in contrast with that linear precursor polymer *l*-P_6-10 exhibited no detectable molecular ionic peak at *m/z* larger than 4,000. The concentrated peaks and signal enhancement in the lower molar mass region is due to general mass discrimination effect of MALDI-TOF-MS measurements,[6] such distinct difference in higher molecular weight molecular ionic segments beyond 3,000 between cyclic polymer *c*-P_6-10 and its linear precursor *l*-P_6-10 can be ascribed to their topology influence. It is obvious that cyclic polymers as compared with their linear counterparts will

possess higher probability to retain larger segments of high molecular weights during MALDI fracture process considering their endless ring structure and persisting long chain of the same molar mass upon being primarily fragmented, thus the difference as presented in Figure S6 serves as an indirect evidence for the macrocyclic topological structure.

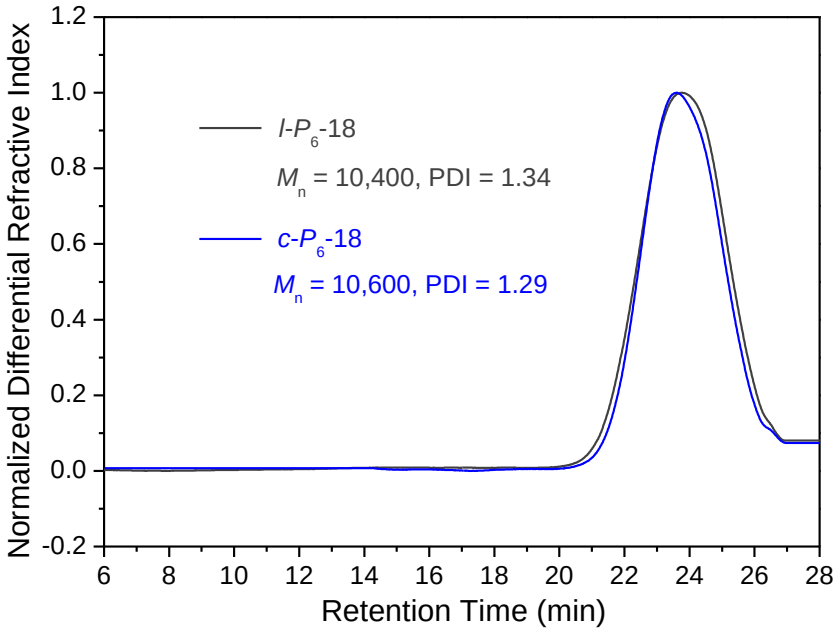

Figure S7. GPC curves comparison of cyclic polymer *c*-P_6-18 and its linear precursor *l*-P_6-18

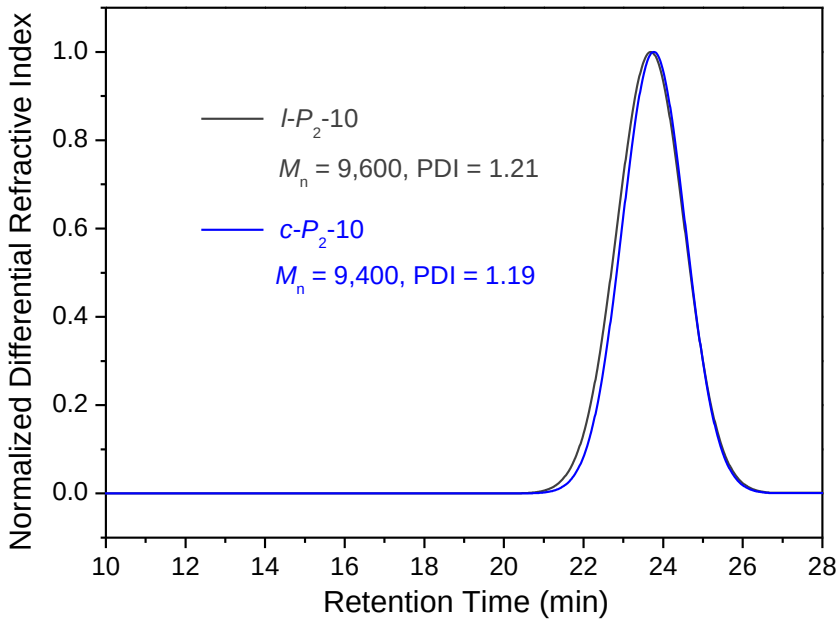

Figure S8. GPC curves comparison of cyclic polymer *c*-P_2-10 and its linear precursor *l*-P_2-10

5. Verification of the cyclic structure via post ring-opening reaction

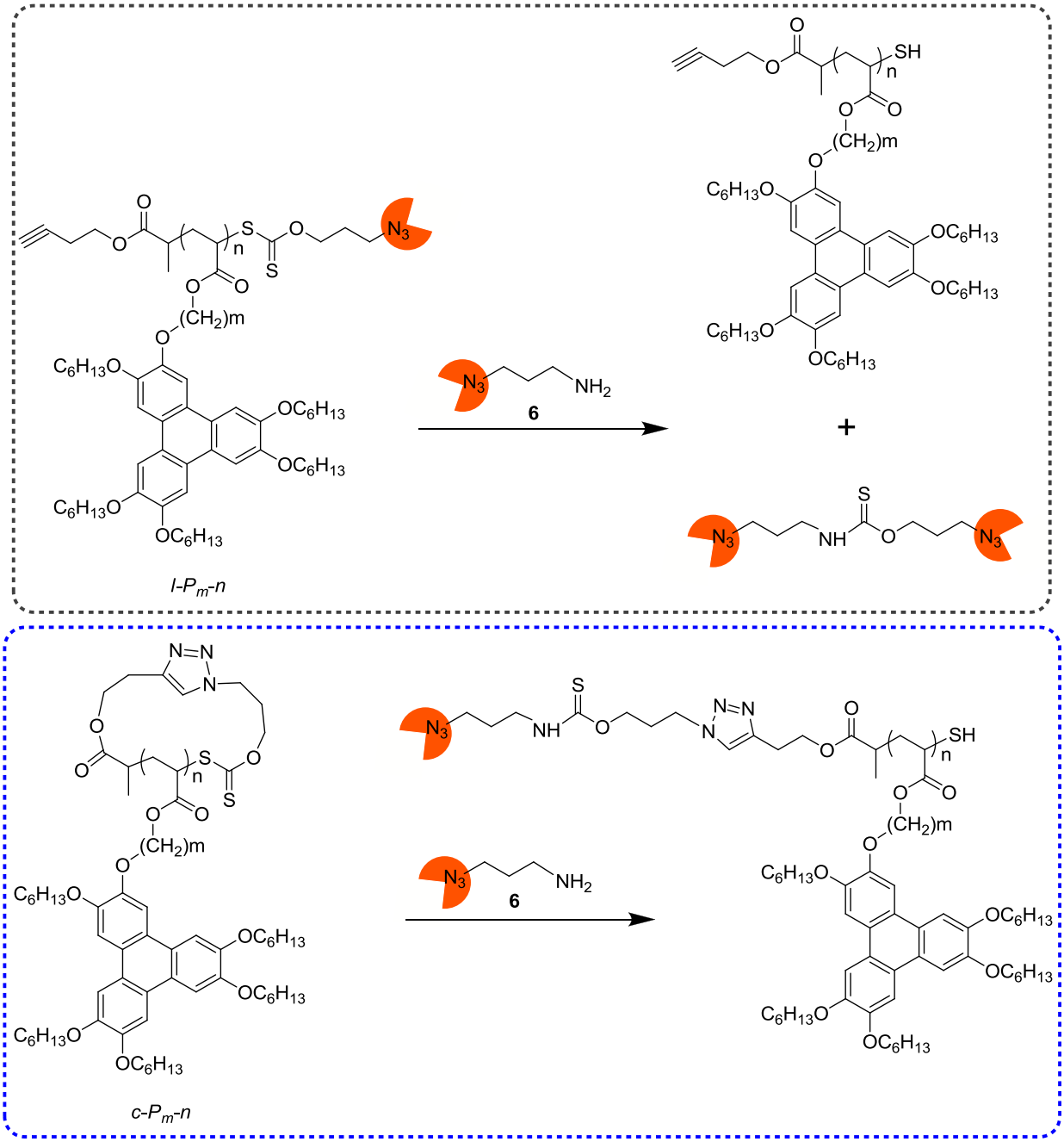

Scheme S3. The aminolysis route and product comparison of linear precursor *l*-P_m-*n* and cyclic polymer *c*-P_m-*n* with an azide-containing amine reagent†.

†The functional amine reagent 3-azido-1-propylamine (**6**) was synthesized according to the literature procedure.[7]

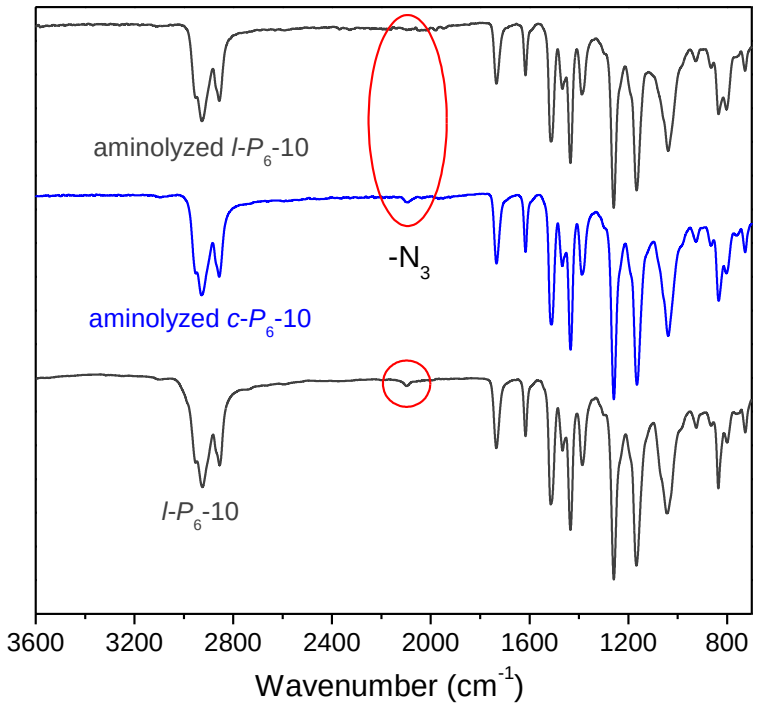

Figure S9. FT-IR spectra of polymer products after aminolyzing the thioester of linear polymer *l*-P_6-10 and cyclic polymer *c*-P_6-10 with azide functionalized amine, also with the FT-IR spectrum of precursor linear polymer *l*-P_6-10 for comparison.

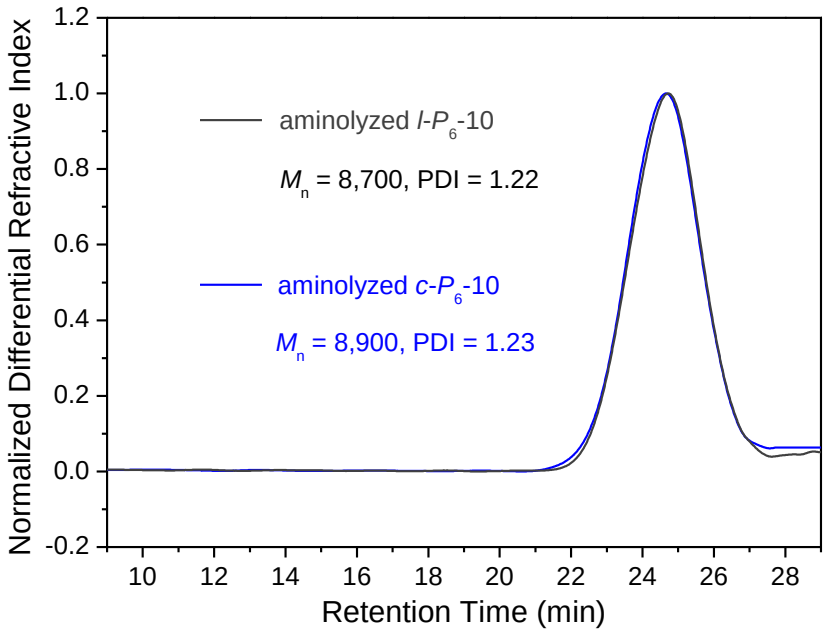

Figure S10. GPC traces comparison of polymer products after aminolysis of linear polymer *l*-P_6-10 and cyclic polymer *c*-P_6-10.

The thioester bond within the polymer product obtained through RAFT polymerization can be

cleaved through aminolysis, which is usually utilized to transform or eliminate the hazardous thioester for biological applications.[8] Herein we adopted a functionalized amine, an azide-containing reagent of 3-azido-1-propylamine (**6**), which can aminolyze thioester well and make a distinction between linear and cyclic polymers. As illustrated in Scheme S3, after aminolysis with the azide-functionalized amine the original azide end group of linear polymer *l*-P_6-10 will be eliminated as a thiourethane byproduct and obtain an azide-absent polymer, while the azide end group will be introduced into the aminolyzed product of cyclic polymer *c*-P_6-10 after ring opening aminolysis reaction. As shown in Figure S9 a 2098 cm^{-1} absorption band characteristic of azide clearly appears in the FT-IR spectrum of aminolyzed polymer product from cyclic *c*-P_6-10 while absent in that from linear polymer *l*-P_6-10, just the opposite case as compared with the FT-IR spectra shown in Figure 2 of main text for the original cyclic *c*-P_6-10 and linear *l*-P_6-10 polymers, which further validates the ring structure of cyclic polymers. And moreover, we also analyzed the aminolyzed polymer products by GPC. As shown in Figure S10, the GPC traces of aminolysis polymer products from either cyclic or linear polymers appear to be nearly the same, also highly similar to that of original *c*-P_6-10 and *l*-P_6-10 as presented in Figure 2 of main text, which is not unexpected considering the quite little molecular weight change with a small molecular segment attached or removed as shown in Scheme S3. In addition, it is also demonstrated that here the end-group effect on GPC performance is insignificant, since different combinations of variant terminal groups of azide, alkyne and thiol with or without triazole linkage are broadly involved in the linear precursor polymer or aminolyzed polymer products.

6. Structural characterization results comparison of *c*-P_m-*n* and *l*-P_m-*n*

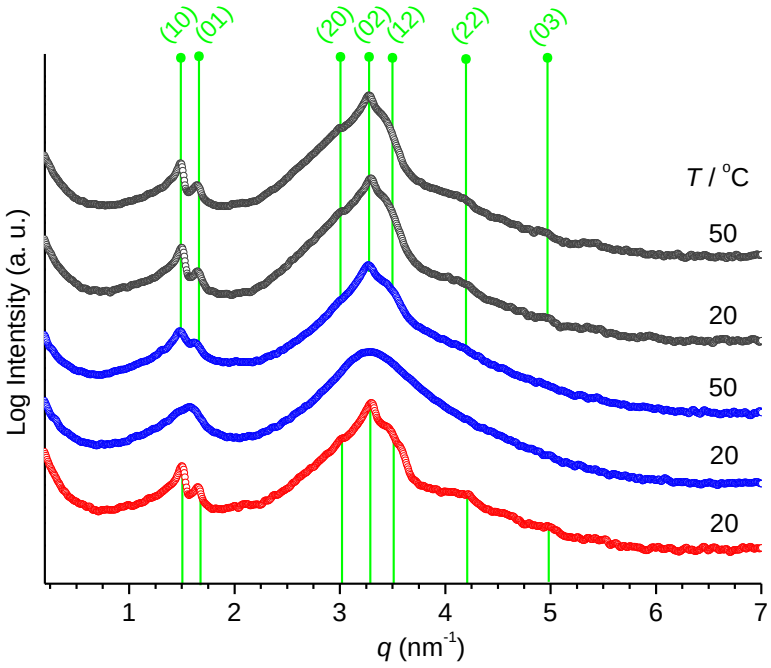

Figure S11. Variable temperature SAXS patterns comparison of cyclic polymer *c*-P_6-10 (blue) and its linear counterpart *l*-P_6-10 (dark grey) with proposed indexing at indicated temperatures during the subsequent heating process after cooling from isotropic melts at 10 ℃ min^{-1}, and the curve in red indicating the cyclic polymer *c*-P_6-10 sample after slowly cooling from the isotropic melt.

Table S1. SAXS/WAXS data for precursor linear polymer *l*-P_6-10 at 20 °C after cooling from isotropic state at 10 °C min^{-1}.

mesophase	*hkl*	d_{obs} [Å]	d_{cacl} [Å]	lattice parameter [Å]	ρ_{calc} [a]
$Col_{ob\text{-}s}$	100	41.9	41.9	a = 42.1	1.07 g cm^{-3}
(20 °C)	010	37.9	37.9	b = 38.0	
*p*2	200	20.9	20.9	γ = 84.4°	
	020	18.9	18.9		
	120	18.0	17.9		
	220	14.8	14.9		
	030	12.6	12.6		
		4.4 (diffuse halo)			
	001	3.51			

[a] The density, ρ, was calculated as $\rho = M \cdot Z/(N_A \cdot V_{unit\ cell})$, where $V_{unit\ cell} = a \cdot b \cdot \sin\gamma \cdot c$, M is the molecular weight of the repeat unit of 899 g mol^{-1}, and Z = 4 (c = 3.51 Å).

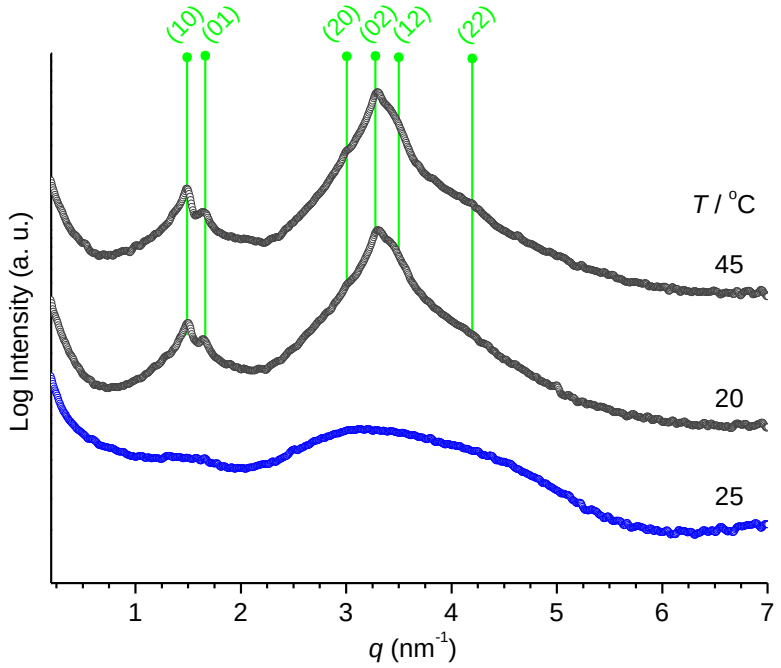

Figure S12. Variable temperature SAXS patterns comparison of cyclic polymer *c*-P_6-18 (blue) and its linear counterpart *l*-P_6-18 (dark grey) with proposed indexing at indicated temperatures during the subsequent heating process after cooling from isotropic melts at 10 °C min^{-1}.

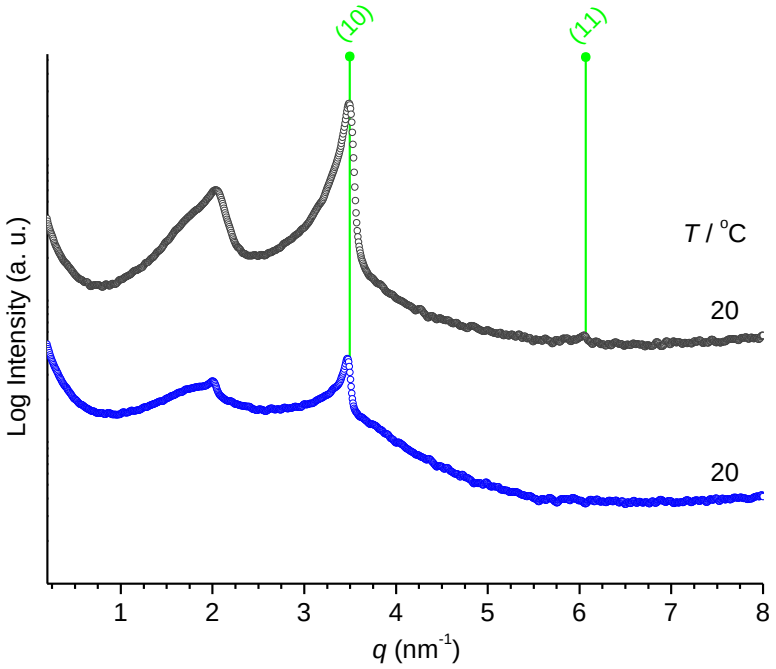

Figure S13. Variable temperature SAXS patterns comparison of cyclic polymer *c*-P_2-10 (blue) and its linear counterpart *l*-P_2-10 (dark grey) with proposed indexing at 20 ℃ after cooling from isotropic melts at 10 ℃ min^{-1}.

Table S2. SAXS/WAXS data for precursor linear polymer *l*-P_2-10 at 20 ℃ after cooling from isotropic state at 10 ℃ min^{-1}.

mesophase	*hkl*	d_{obs} [Å]	d_{cacl} [Å]	lattice parameter [Å]	ρ_{calc} [a]
Col_{ho}	100	18.0	18.0	a = 20.8	1.06 g cm^{-3}
(20 ℃)	110	10.4	10.4		
*p*6*mm*		4.4 (diffuse halo)			
	001	3.54			

[a] The density, ρ, was calculated as $\rho = M \cdot Z/(N_A \cdot V_{unit\ cell})$, where $V_{unit\ cell} = a^2 \cdot c \cdot \sqrt{3}/2$, M is the molecular weight of the repeat unit of 843 g mol^{-1}, and Z = 1 (c = 3.54 Å).

7. UV-vis absorption spectra comparison of *c*-P_m-*n* and *l*-P_m-*n*

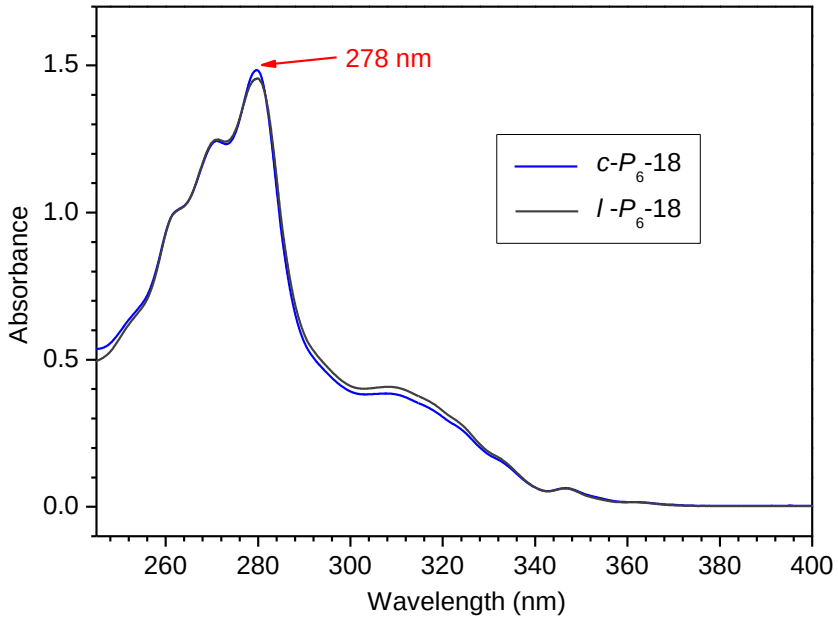

Figure S14. Representative UV-vis absorption spectra comparison of cyclic polymer *c*-P_6-18 and its linear precursor *l*-P_6-18 in CH_2Cl_2 solution with concentration 0.02 g L^{-1}.

8. References for supplementary information

1 B. Mu, B. Wu, S. Pan, J. L. Fang and D. Z. Chen, *Macromolecules*, 2015, **48**, 2388-2398.

2 B. Mu, S. Pan, H. F. Bian, B. Wu, J. L. Fang and D. Z. Chen, *Macromolecules*, 2015, **48**, 6768-6780.

3 A. A. Kislukhin, V. P. Hong, K. E. Breitenkamp and M. G. Finn, *Bioconjugate Chem.*, 2013, **24**, 684-689.

4 F. Carta, A. Akdemir, A. Scozzafava, E. Masini and C. T. Supuran, *J. Med. Chem.*, 2013, **56**, 4691-4700.

5 M. Alijanianzadeh, A. A. Saboury, H. Mansuri-Torshizi, K. Haghbeen and A. Moosavi-Movahedi, *J. Enzyme Inhib. Med. Chem.*, 2007, **22**, 239-246.

6 G. Montaudo, F. Samperi and M. S. Montaudo, *Prog. Polym. Sci.*, 2006, **31**, 277-357.

7 J. Hannant, J. H. Hedley, J. Pate, A. Walli, S. A. F. Al-Said, M. A. Galindo, B. A. Connolly, B. R. Horrocks, A. Houlton and A. R. Pike, *Chem. Commun.*, 2010, **46**, 5870-5872.

8 H. Willcock and R. K. O'Reilly, *Polym. Chem.*, 2010, **1**, 149-157.